# Energy & Environmental Science

Accepted Manuscript






ROYAL SOCIETY OF CHEMISTRY

www.rsc.org/ees

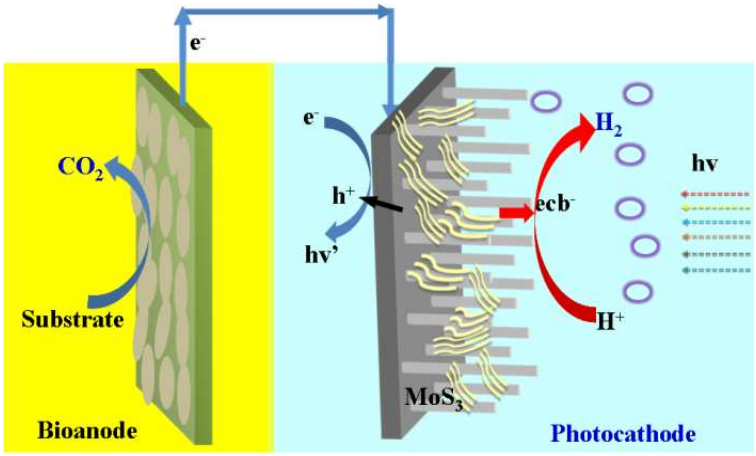


A bio-photoelectrochemical cell with a bioanode and a $MoS_3$/SiNW photocathode is successfully constructed for hydrogen production under visible light illumination

# Bio-photoelectrochemical cell with $MoS_3$-modifed silicon nanowire photocathode for hydrogen and electricity production

Guo-Long Zang, Guo-Ping Sheng*, Chen Shi, Yun-Kun Wang, Wen-Wei Li, Han-Qing Yu*

Department of Chemistry, University of Science and Technology of China, Hefei, 230026, China

*** Corresponding authors**:

Guo-Ping Sheng, Tel: +86-551-63607453, Fax: +86-551-63601592; E-mail: gpsheng@ustc.edu.cn;

Han-Qing Yu, Tel: +86-551-63607592, Fax: +86-551-63601592; E-mail: hqyu@ustc.edu.cn

## Abstract

Hydrogen production by solar energy conversion is an attractive and promising sustainable energy technology. Tremendous research effort has been directed towards the development and application of photoelectrochemical cell for hydrogen generation. Here, we report a novel bio-photoelectrochemical cell, which is consisted of a $MoS_3$ modified p-type Si nanowire photocathode and a microbially-catalyzed bioanode, for hydrogen production under visible light illumination. Microbial pollutant oxidation occurs spontaneously in the bioanode, which provides sufficient electrons for the photocathode reaction without external bias. The recombination of the photogenerated holes ($h_{vb}^{+}$) and electrons ($e_{cb}^{-}$) pairs at the photocathode is retarded by the supply of electrons from the bioanode, leaving more available photogenerated electrons for hydrogen evolution reactions. As a result, the hydrogen production performance is improved. Under light illumination, hydrogen is continuously produced from the bio-photoelectrochemical cell, with a maximum power density of 71 mW $m^{-2}$ and an average hydrogen-producing rate of 7.5±0.3 μmol $h^{-1}$ $cm^{-2}$.

## Broader context

Here, a new concept bio-photoelectrochemical cell is constructed for hydrogen production, which is composed of a $MoS_3$ modified silicon nanowire photocathode and a microbially-catalyzed bioanode. The results provide solid evidence that the electrons coming from microbes could be used as an efficient reducing agent for the semiconductor photocathode. The recombination of the photogenerated holes and electrons at the photocathode is retarded by the supply of electrons from the bioanode, and thus the hydrogen production performance is improved. Such a bio-photoelectrochemical cell can be used for a wide range of processes, such as pollutant degradation and hydrogen production, and deserves further investigations.

## Introduction

Photoelectrochemical water splitting has attracted great interests as an effective way of converting sunlight into chemical energy in the form of hydrogen, which is a clean alternative to fossil fuel.[1-5] Especially, extensive research efforts have been directed towards the development of photoelectrochemical cells for hydrogen generation with semiconductor photocathodes.[6, 7] Nevertheless, in such systems, a larger bias is often used to overcome the overpotentials associated with the hydrogen and oxygen evolution reaction.[7-9] It has been reported that splitting water into oxygen and hydrogen could be achieved without applying an external voltage through combining a n-type semiconductor photoanode and a p-type semiconductor photcathode under UV or visible light illumination.[10, 11] However, due to the high material costs and the shortage of suitable semiconductors, so far limited progress has been made on this aspect.

Bioelectrochemical systems are effective for the production of energy and value-added products such as fuels and chemicals.[12-14] In a bioelectrochemical system, bacteria oxidize organic substrates and deliver the released electrons from bacterial cells to anode, and then the electrons are conducted through the external circuit to the cathode.[15] At cathode, protons, carbon dioxide or acetate are reduced to hydrogen peroxide, hydrogen, methane or ethanol by electrons, but an external voltage is typically needed to overcome the thermodynamic barrier.[16-19] This has greatly constrained its development and practical application. Solar energy can sever as a substitute. However, the question remains whether a semiconductor is used as cathode, and the electrons generated from bioanode can be combined with the generated holes

to promote photocathode performance under light illumination spontaneously. A previous study reported that a system coupling a bioanode with a $Cu_2O$ photocathode only gave a low level of current and no hydrogen production was obtained.[20] Thus, investigations into how to couple the bioanode and photocathode efficiently with appropriate photocatalysts for hydrogen production are highly desired.

Silicon is the most abundant semiconductor and widely used in photovoltaic devices, and has high visible-light-absorption capability.[21, 22] It is a promising material for photocathode in a photoelectrochemical system for hydrogen production.[23] However, to achieve a high production efficiency, co-catalysts for the hydrogen evolution reaction (HER) are required. In this context, noble metals like platinum (Pt) are usually used because of their high activity for HER, but their high costs and scarcity have hindered their practical applications.[24] Thus, abundant non-precious-metal alternatives are highly desired. Previous studies have demonstrated that $MoS_2$ and $Mo_3S_4$ clusters could serve as an efficient co-catalyst to catalyze the HER at a photocathode.[25, 26] In the present study, a cost-effective HER photocathode was prepared through depositing amorphous $MoS_3$ onto silicon nanowire (SiNW) electrode, and the amorphous $MoS_3$ was found to act as an efficient, robust and earth-abundant co-catalyst of SiNW to catalyze the HER.

In this paper, we report a new self-sustained bio-photoelectrochemical cell (BPEC) (Figure S1 in the Supporting Information), which is composed of a $MoS_3$ modified SiNW ($MoS_3$/SiNW) photocathode and a microbially-catalyzed bioanode, for hydrogen production. The results may be useful for designing new systems for

hydrogen production from solar energy.

## Materials and methods

**Electrode preparation.** SiNW was fabricated by a metal-catalyzed electroless etching of bulk Si samples.[27] Single-crystal B-doped silicon (100) wafers (projected surface area 6 $cm^2$, thickness 0.6 mm, resistivity 0.005-0.05 Ω cm) was degreased by rinsing with acetone, ethanol and deionized water in sequence. After that, the Si surface was immersed into a piranha solution (1:3 v/v 30% $H_2O_2$: concentrated $H_2SO_4$) for 10 min and then immersed into 5% HF for 2 min to strip off the silicon oxide on the surface. For metal-catalyzed electroless etching, the Si sample was immersed in 0.02 M $AgNO_3$ and 3.6 M HF for 60 min. Then, the Si sample was immersed in diluted $HNO_3$ for 1 h to remove residual Ag seed. Prior to $MoS_3$ deposition, the Si-NW electrodes were cleaned by 5 wt% HF solution to remove the $SiO_2$ layer. The obtained H-terminated Si electrode was rinsed with pure water and transferred into the photoelectrochemical cell for further experiments.

**Deposition of $MoS_3$:** Deposition was performed according to the work of Merki et al.[28] The electrolyte was composed of 2 mM $(NH_4)_2(MoS_4)$ and 0.1 M $NaClO_4$. Thirty consecutive cycles of CV were carried out on a CHI660C electrochemical workstation (Chenhua Instrument Co., China) with a Ag/AgCl reference electrode (0.2 V vs SHE, Wuhan Gaoss Union Sci. Instru. Co., China) and a Pt wire counter electrode. The CV was performed with potential from +0.1 to -1.0 V vs. Ag/AgCl at a scan rate of 0.05

111 V $s^{-1}$. Then, the modified electrode was thoroughly rinsed with distilled water and
112 used as the photoelectrode. The conduction band of B-Si wafer is around -0.21 eV,
113 and that of $MoS_3$ is about -1.12 eV (determined from UV-visible absorption spectra
114 and Mott-Schottky plots).
115
116 **Reactor construction and operation.** In this study, a double-chamber BPEC with a
117 working volume of 215 mL was used for the tests (Figure S1). The anode chamber
118 and the cathode chamber were made of glass and quartz glass, respectively, and the
119 two chambers were separated by a 6.6 $cm^2$ anion exchange membrane (Ultrex
120 AMI7001, Membranes International Inc., US). The anodic chamber was filled with
121 granular graphite of 3-5 mm size (Beijing Sanye Carbon Co., China), which was used
122 as anode. Graphite felt (16 $cm^2$, without wet proofing, Beijing Sanye Carbon Co.,
123 China) was used in the anodic compartments to connect electrode to the external
124 circuit. All the graphite granules were washed at least three times with distilled water
125 before being immersed overnight in 1 M NaOH and 1 M HCl in turn. Afterwards, the
126 granules were washed three times with distilled water. During the cultivation of
127 electrochemically active bacteria in the bioanode, the carbon felt without wet proofing
128 was initially used as the cathode (with a projected surface area of 16 $cm^2$). The
129 cathode compartment (50 mM phosphate buffer solution, pH 7.0) was continuously
130 sparged with air in experiments where oxygen was used as the electron acceptor. After
131 the output voltage reached above 300 mV (with an external resistance of 500 Ω) and
132 became stabilized (Figure S2 in the Supporting Information shows the variations of

voltage during the long-term operation and the polarization curves), the bioanode was used to couple with the photocathode of the BPEC. Then, the cathode electrode was replaced by the $MoS_3$ modified SiNW electrode, and the catholyte was changed to a solution mixture of $H_2SO_4$ +0.5 M $K_2SO_4$ (pH 1.0) for hydrogen production.

The anode chamber of BPEC was continuously fed with substrate in an upflow mode through a peristaltic pump (Lange Co., China). The influent flow rate was 20 mL $h^{-1}$. The substrate was consisted of (in 1 L of 50 mM phosphate buffer solution, pH 7.0): $CH_3COONa \cdot 3H_2O$, 1400 mg; $NH_4Cl$, 310 mg; KCl, 130 mg; $CaCl_2$, 10 mg; $MgCl_2 \cdot 6H_2O$, 20 mg; NaCl, 2 mg; $FeCl_2$, 5 mg; $CoCl_2 \cdot 2H_2O$, 1 mg; $MnCl_2 \cdot 4H_2O$, 1 mg; $AlCl_3$, 0.5 mg; $(NH_4)_6Mo_7O_{24}$, 3 mg; $H_3BO_3$, 1 mg; $NiCl_2 \cdot 6H_2O$, 0.1 mg; $CuSO_4 \cdot 5H_2O$, 1 mg; $ZnCl_2$, 1 mg.

The anaerobic microorganisms for the BPEC inoculation were collected from a full-scale upflow anaerobic sludge blanket reactor in Bengbu City, China. After acclimation, appropriate electrochemically active bacteria on the electrode would be selected as reported previously,[29] evidenced by the SEM images of the anode-attached microorganisms (Figure S3 in the Supplementary Information).

**Photoelectrochemical measurement.** In order to evaluate the photocathode performance, the response of current to potential under illumination was measured by using a three electrode cell with the photocathode as the working electrode, a Pt wire counter electrode and a Ag/AgCl reference electrode. To measure the response of current to potential under continuous illumination, a much higher scan rate of 100

mV/s was adopted to obtain the photocurrent profiles as a function of potential. However, in the tests under chopped illumination, manual shielding/unshielding of light was adopted, which necessitates a relatively long scanning time. In this case, a moderate scan rate of 10 mV/s was chosen to better show the variation of light response.

Linear sweep voltammetry was used to obtain the polarization curves using a CHI660C electrochemical workstation (Chenhua Instrument Co., China) in one typical cycle at a scan rate of 1 mV $s^{-1}$.[30] The polarization curves of the BPEC were measured in a two electrode system, where the anode served as the working electrode and the cathode as the counter and reference electrodes. The voltage and power were obtained as a function of current density, and normalized to the photocathode area.

The output voltage of the BPEC across an external resistor (V) was measured and recorded using a data acquisition system (Agilent 34970A, Agilent Co., USA) connected to a computer. The current ($I$) was calculated according to Ohm's law, $I = V/R$, where $R$ is the external resistance. The power ($P$) was calculated from $P=I\times V$.

The $H_2SO_4$ +0.5 M $K_2SO_4$ (pH 1.0) aqueous solution was used as electrolyte for photoelectrochemical measurements. A 350 W Xe lamp (PLS-SXE-300UV, Beijing Trusttech Co., China) with a 420 nm cut-off filter were used as a visible-light source (The intensity of light was about 120 W/$m^2$). The amount of evolved $H_2$ was determined by gas chromatography (SP-6890, Lunan Co., China). The total hydrogen amount produced was calculated by multiplying the hydrogen content in 1-mL gas sample with the headspace volume of the BPEC cathode chamber (75 mL). The

charge balance was calculated based on the total amount of electrons from the external electric circuit and the amount required by the cathode for hydrogen production.

**Cathode characterization.** The morphology of the cathode samples was imaged with scanning electronic microscopy (SEM, Sirion200, FEI Ltd., UK). X-ray photoelectron spectroscopy (XPS) measurement was applied to determine the surface composition using an ESCALAB 250 instrument (Thermo Fisher Scientific Inc, USA). The XPS spectra were analyzed and fitted using curve-fitting software (XPSPEAK v4.0).

## Results and discussion

**Preparation and characterization of $MoS_3$/SiNW photoelectrode**. Figure 1A shows a typical SEM image of the SiNW array fabricated through metal-assisted chemical etching of p-type Si (100). The images show that the surface of the Si electrode was covered by dense and well-aligned nanowires with uniform distribution, similar to those described previously.[21, 27] Figure 1B illustrates the SEM images of a $MoS_3$-modified SiNW electrode produced using cyclic voltammetry. The $MoS_3$ particles clustered together at the surface of SiNW electrode, and made the surface rough. XPS analysis was used to collect more information concerning the structure and chemical states of the electrodeposited $MoS_3$. The characteristic peaks of Mo, S, Si and O were observed in the XPS spectrum (Figure S4 in the Supporting

Information). The binding energy of Mo 3d in the electrode was 229.4 eV, confirming that the Mo ion was in +4 oxidation state. The Mo 3d signal shows the characteristic doublet of Mo $3d^5$ and Mo $3d^3$ at binding energies of 229.4 and 232.6 eV, respectively. The binding energies of the Mo atom in the electrode were identical to those of a thermally prepared $MoS_3$ sample.[31] The contribution of the S 2s, at a binding energy of 226.6 eV, was obvious on the low binding energy side of the Mo 3d signal (Figure 1C). The S 2p spectrum in Figure 1D shows two peaks with S 2p energies of 162.4 and 163.5 eV, suggesting the presence of both $S^{2-}$ and $S_2^{2-}$ ligands.[28] The peak at 162.4 eV was likely to be the sulfur ions, and another with a higher binding energy should be attributed to $S_2^{2-}$ ions.[31] The binding energies of the S atom in the electrode were similar to those of amorphous $MoS_3$.[32]

**Photoelectrocatalytic activity of $MoS_3$/SiNW photoelectrode.** The catalytic activity of the modified electrode was evaluated in the solution of $H_2SO_4$ + 0.5 M $K_2SO_4$ (pH 1.0). Figure 2A shows the linear sweep voltammagrams recorded from the photocathode in the dark and under visible light. Almost no current could be produced in the dark, while the electrode exhibited a photocurrent up to 1.5 mA $cm^{-2}$ at -0.2 V (vs Ag/AgCl) under light illumination. The electrode was highly photoelectrochemically active (Figure 2B). Notably, the onset potential of the photoelectrode reached approximately +0.10 V vs Ag/AgCl under light illumination, which was more positive than that of the SiNW without $MoS_3$ catalyst.[25, 27] Different scanning rates were adopted to measure the response of current to potential under

continuous and chopped light illuminations. Such a difference in scanning rate resulted in the different photocurrents in Figure 2a and b. The results indicate that, $MoS_3$ could be used as an efficient co-catalyst of the SiNW arrays to accelerate the HER. Furthermore, the catalyst was also stable after illumination, evidenced by the CV of the $MoS_3$-SiNW electrode in dark and light (Figure S5).

**Effect of illumination on cell performance.** To evaluate the influence of illumination on the BPEC performance, the BPEC voltage across a 52.4 ohm resistor and the cathode potential were recorded at 1 s interval (Figure 3). During the 4000 s of light and dark cycles, both voltage generation and cathode potential increased under light and decreased in the dark. The voltage loss would occur due to the presence of the internal resistance. Since the anode chamber was operated in a continuous mode at a constant flow rate, the bioanode potential of BPEC was relatively stable. Thus, the variation of power production was caused by a varied potential of the cathode.

Furthermore, the effect of illumination on the power output in BPEC was examined. As shown in Figure S6, the maximum current density of the bioanode was much higher than that of the photocathode. This indicates that the number of electrons transferred from the bioanode was much more than the number of the photogenerated holes at the cathode, suggesting that bioanode could ensure an appropriate level of electrons for the cathode reaction. Figure 4 shows the power density curves of the BPEC operated under illumination and in the dark. The maximum power density reached 71 mW $m^{-2}$ with a current density of 0.69 A $m^{-2}$ under light illumination,

243 implying that the electricity could be readily generated from the BPEC under
244 illumination.
245
246 **Electricity generation and hydrogen production.** In the hydrogen-producing
247 experiments, the two chambers were purged with $N_2$ to ensure the anaerobic
248 conditions and then sealed, and the gas composition was monitored in the whole
249 cycles. No oxygen was detected in any gas samples, and hydrogen was continuously
250 produced in the cathode chamber. The electricity was produced when the electrons
251 from the bioanode migrated through the external circuit to combine with the
252 photogenerated holes of the photocathode. As illustrated in Figure 5A, current was
253 generated in response to light. Meanwhile, the produced hydrogen increased almost
254 linearly over time under illumination (Figure 5B). The average hydrogen-producing
255 rate reached 7.5±0.3 μmol $h^{-1}$ $cm^{-2}$ (normalized to the cathode area) in the three cycles.
256 For comparison, under open circuit conditions, the hydrogen production rate was
257 significantly reduced to 2.2±0.1 μmol $h^{-1}$. On the other hand, in the dark, the current
258 and hydrogen production was negligible. These results indicate that light illumination
259 was essential for the current and hydrogen generation in such a cell, and the bioanode
260 and photocathode could work synergetically to promote the electricity and hydrogen
261 production.
262
263 **Discussion**

Although a system coupling a bioanode with a $Cu_2O$ photocathode was constructed in a previous work,[17] we have, for the first time, provided experimental evidence about the successful operation of a self-sustained BPEC with a $MoS_3$-modified SINW electrode for spontaneous hydrogen and electricity generation under visible light illumination. The experimental results clearly demonstrate that electricity generation and hydrogen production could be achieved in a self-bias BPEC with a microbial anode and a specifically designed photocathode. In this BPEC, two half-reactions are involved (Figure 6): the organics oxidized by the microorganisms in the anode (Reaction 1) and proton reduction in the cathode (Reactions 2-4).

$$CH_3COO^- + 2H_2O \rightarrow 2CO_2 + 7H^+ + 8e^- \quad (1)$$

$$MoS_3/SiNW + hv \rightarrow h_{vb}^+ + e_{cb}^- \quad (2)$$

$$e^- + h_{vb}^+ \rightarrow hv' \quad (3)$$

$$2H^+ + 2e_{cb}^- \rightarrow H_2 \quad (4)$$

The oxidation of organics by the microorganisms in the bioanode (Reaction 1) occurs spontaneously, which provides sufficient electrons to continuously transport to the cathode through the external circuit without external bias.[33] At the photocathode, $h_{vb}^+$ and $e_{cb}^-$ are produced under illumination (Reaction 2). The electrons coming from Reaction 1 are captured by the holes in the valence band of the photocathode (Reaction 3). As a result, the recombination of photogenerated carriers is efficiently reduced. The photocatalytic efficiency and hydrogen production attributed to the reduction of protons by $e_{cb}^-$ are greatly improved (Reaction 4).

The above reactions are affected by each other. For example, the electrons coming from Reaction 1 can greatly accelerate Reaction 4. However, if Reaction 2 does not occur (e.g., in the dark), the electrons from Reaction 1 could not be transferred to the photocathode, and there would be no power output and less hydrogen production in the cell. The photo-excited electrons are immediately combined with the protons, while the holes are trapped by the electrons supplied from the bioanode. Thus, the photo-generated electrons and holes are efficiently dissociated, and the photocatalytic efficiency and hydrogen production can be greatly improved. In this case, the electrons from the bioanode could serve as an efficient reducing agent for the hydrogen-producing photocathode.

In order to transfer the electrons from the bioanode to the photocathode effectively, the cathode potential must be higher than the anode potential. The proton reduction in the SiNW electrode has a very low redox potential and high overpotential, as reported previously.[25-27, 34] Thus, the use of protons as electron acceptor would result in a very low voltage production. However, in the presence of $MoS_3$ on the SiNW surface, the onset potential was greatly enhanced and the overpotential for hydrogen generation was significantly reduced. As a result, continuous hydrogen generation from the BPEC was achieved. Therefore, the reduction overpotential of HER on the electrode surface could be further reduced through electrode preparation and modification, which would lead to more efficient energy production.

In addition, in the 4000-s light and dark cycles (Figure S7), the voltage generation of a control system with the abiotic-anode and photocathode also increased

under light and decreased in the dark. However, compared with the BPEC, its voltages were much smaller. This result clearly indicates that both the microbial anode and photocathode were indispensable. The synergetic functions of the microbial anode and photocathode in our system should be taken into account. In the BPEC, a low pH of the catholyte was applied in order to increase the cathode potential. Thus, an acidic catholyte was beneficial for elevating the current and increasing the combination of the anode-derived electrons with the photo-generated holes. As a consequence, an efficient hydrogen production at the cathode of the BPEC was achieved in our system. Thus, to ensure stable hydrogen production in the BPEC system, a relatively acidic catholyte pH should be maintained. The BPEC could also be used for treating acidic wastewaters (e.g., from mining industry) at the cathode chamber. The low pH and usually high conductivity of such streams might favor a good cathode performance of the BPEC. These strategies might make the BPEC process sustainable, although the true performances of such systems are still to be experimentally evaluated.

Aside from net energy production, the BPEC also has advantages in term of costs than conventional photoelectrochemical systems. Because of the use of bioanode in the BPEC, an external bias and use of Pt catalyst at the anode that is essential in conventional photoelectrochemical cell can be avoided. Moreover, the low-cost $MoS_3$/SiNW photocathode, instead of conventional semiconductors and Pt, was used for reduction of proton to hydrogen. As a result, the hydrogen-production cell is cost-effective, energy-saving and environmentally friendly, compared with the

conventional photoelectrochemical systems.[35, 36] In addition, because of the diversity of the microbial communities in the anode, various types of substrates, including wastewater, pollutants and lignocellulosic biomass, could be used for substrate to produce electrons.[37] Thus, the BPEC can be used for a wide range of processes such as pollutant degradation and fuel production, and it deserves further investigations.

**Acknowledgements**

The authors wish to thank the National Hi-Technology Development 863 Program of China (2011AA060907), NSFC (51322802), and the Program for Changjiang Scholars and Innovative Research Team in University of Ministry of Education of China for the partial support of this study.

**References**

1 A. Fujishima, K. Honda, *Nature,* 1972, **238**, 37-38.

2 J.A. Turner, *Science,* 2004, **305**, 972-974.

3 A. Paracchino, V. Laporte, K. Sivula, M. Gratzel, E. Thimsen, *Nat. Mater.,* 2011, **10**, 456-461.

4 J.R. Bolton, *Sol. Energy,* 1996, **57**, 37-50.

5 M. Momirlan, T. Veziroglu, *Renew. Sust. Energ. Rev.,* 1999, **3**, 219-231.

6 M. H. Lee, K. Takei, J. J. Zhang, R. Kapadia, M. Zheng, Y. Z. Chen, J. Nah, T. S. Matthews, Y. L. Chueh, J. W. Ager, A. Javey, *Angew. Chem. Int. Edit.,* 2012, **51**, 10760-10764.

7 M. G. Walter, E. L. Warren, J. R. Mckone, S. W. Boettcher, Q. X. Mi, E. A. Santori, N. S. Lewis, *Chem. Rev.,* 2010, **110**, 6446-6473.

8 F. E. Osterloh, *Chem. Soc. Rev.,* 2013, **42**, 2294-320.

9 P. Lianos, *J. Hazard. Mater.,* 2011, **185**, 575-590.

10 H. L. Wang, T. Deutsch, J. A. Turner, *J. Electrochem. Soc.,* 2008, **155**, F91-F96.

11 S. Ida, K. Yamada, T. Matsunaga, H. Hagiwara, Y. Matsumoto, T. Ishihara, *J. Am. Chem. Soc.,* 2010, **132**, 17343-17345.

12 T. H. Pham, P. Aelterman, W. Verstraete, *Trends Biotechnol.,* 2009, **27**, 168-178.

13 P. Clauwaert, P. Aelterman, T. H. Pham, L. D. Schamphelaire, M. Carballa, K. Rabaey, W. verstraete, *Appl. Microbiol. Biot.,* 2008, **79**, 901-913.

14 X. W. Liu, W. W. Li, H. Q. Yu, *Chem. Soc. Rev.*, 2014, DOI: 10.1039/C3CS60130G

15 D. Pant, D. Arslan, G. Van Bogaert, Y. A. Gallego, H. De Wever, L. Diels, K. Vanbroekhoven, *Environ. Technol.*, 2013, **34**, 1935-1945.

16 B. E. Logan, K. Rabaey, *Science*, 2012, **337**, 686-690.

17 P. Clauwaert, W. Verstraete, *Appl. Microbiol. Biot.,* 2009, **82**, 829-836.

18 K. J. J. Steinbusch, H. V. M. Hamelers, J. D. Schaap, C. Kampman, C. J. N. Buisman, *Environ. Sci. Technol.,* 2010, **44**, 513-517.

19 M. Sharma, N. Aryal, P. M. Sarma, K. Vanbroekhoven, B. Lal, X. D. Benetton, D. Pant, *Chem. Commun.*, 2013, **49**, 6495-6497.

20 F. Qian , G. M. Wang, Y. Li, *Nano Lett.,* 2010, **10**, 4686-4691.

21 A. I. Hochbaum, R. K. Chen, R. D. Delgado, W. J. Liang, E. C. Garnett, M. Najarian, A. Majumdar, P. D. Yang, *Nature,* 2008, **451**, 163-167.

22 S. Y. Reece, J. A. Hamel, K. Sung, T. D. Jarvi, A. J. Esswein, J. J. H. Pijpers, D. G. Nocera, *Science,* 2011, **334**, 645-648.

23 R. N. Dominey, N. S. Lewis, J. A. Bruce, D. C. Bookbinder, M. S. Wrighton, *J. Am. Chem. Soc.,* 1982, **104**, 467-482.

24 Y. Alvarez-Gallego, X. Dominguez-Benetton, D. Pant, L. Diels, K. Vanbroekhoven, I. Genne, P. Vermeiren, *Electrochim. Acta.*, 2012, **82**, 415-426.

25 Y. D. Hou, B. L. Abrams, P. C. K. Vesborg, M. E. Bjorketun, K. Herbst, L. Bech, A. M. Setti, C. D. Damsgaard, T. Pedersen, O. Hansen, J. Rossmeisl, S. Dahl, J. K. Norskov, I. Chorkendorff, *Nat. Mater.,* 2011, **10**, 434-438.

26 P. D. Tran, S. S. Pramana, V. S. Kale, M. Nguyen, S. Y. Chiam, S. K. Batabyal, L. H. Wong, J. Barber, J. Loo, *Chem. Eur. J.,* 2012, *18*, 13994-13999.

27 I. Oh, J. Kye, S. Hwang, *Nano Lett.,* 2012, **12**, 298-302.

28 D. Merki, S. Fierro, H. Vrubel, X. L. Hu, *Chem. Sci.,* 2011, **2**, 1262-1267.

29 X. W. Liu, X. F. Sun, Y. X. Huang, G. P. Sheng, S. G. Wang, H. Q. Yu, *Energ. Environmen. Sci.,* 2011, **4**, 1422-1427.

30 P. Clauwaert, D. V. D. Ha, N. Boon, K. Verbeken, M. Verhaege, K. Rabaey, W. Verstraete, *Environ. Sci. Technol.,* 2007, **41**, 7564-7569.

31 D. Belanger, G. Laperriere, F. Girard, D. Guay, G. Tourillon, *Chem. Mater.,* 1993, **5**, 861-868.

32 T. Weber, J. C. Muijsers, J. W. Niemantsverdriet, *J. Phys. Chem.,* 1995, **99**, 9194-9200.

33 A. ElMekawy, H. M. Hegab, X. Dominguez-Benetton, D. Pant, *Bioresour. Technol.,* 2013, **142**, 672-682.

34 B. Seger, A. B. Laursen, P. C. K. Vesborg, T. Pedersen, O. Hansen, S. Dahl, I. Chorkendorff, *Angew. Chem. Int. Edit.,* 2012, **51**, 9128-9131.

35 J. Turner, G. Sverdrup, M. K. Mann, P. C. Maness, B. Kroposki, M. Ghirardi, R. J. Evans, D. Blake, *Int. J. Energ. Res.,* 2008, **32**, 379-407.

36 K. Christopher, R. Dimitrios, *Energ. Environmen. Sci.* 2012, **5**, 6640-6651.

37 D. Pant, G. V. Bogaert, L. Diels, K. Vanbroekhoven, *Bioresour. Technol.*, 2010, **101**, 1533-1543.

405 **Figure captions**

406

407 **Fig. 1** (A) SEM image of the SiNW electrode fabricated by metal-catalyzed chemical
408 etching; (B) SEM image of the $MoS_3$/SiNW electrode; (C and D) XPS
409 spectra of the $MoS_3$-modified electrode (C: Mo 3d and S 2s region; D: S 2p
410 region)

411 **Fig. 2** (A) Linear sweep voltammagrams of the $MoS_3$/SiNW electrode, the scan rate
412 was 100 mV $s^{-1}$; (B) The transient current responses to on-off cycles of
413 illumination on photocathodes at applied potentials from -0.2 to 0.2 V vs
414 Ag/AgCl with Pt as the counter electrode, the scan rate was 10 mV $s^{-1}$

415 **Fig. 3** Performance of the light-induced BPEC (52.4 Ω of resistor) and photocathode
416 potential change under chopped light illumination

417 **Fig. 4** Polarization (dash line) and power density (solid line) curves of the BPEC in
418 dark (blue curve) and light (red curve), respectively. Polarization curves
419 were determined by performing linear sweep voltammetry with a
420 two-electrode system in one typical cycle. The scan rate was 1 mV $s^{-1}$.

421 **Fig. 5** Current (A) and hydrogen production (B) of the BPEC (across 52.4 Ω resistor)
422 in dark and light.

423 **Fig. 6** Working principle of the BPEC

424

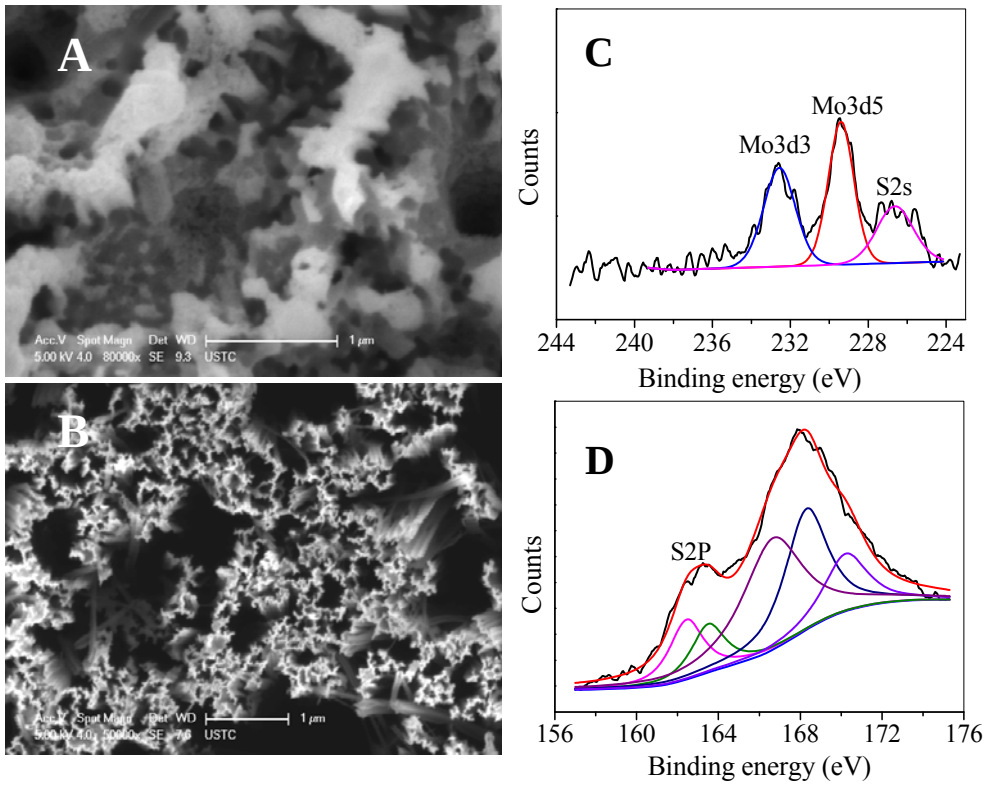


**Fig. 1** (A) SEM image of the SiNW electrode fabricated by metal-catalyzed chemical etching; (B) SEM image of the $MoS_3$/SiNW electrode; (C and D) XPS spectra of the $MoS_3$-modified electrode (C: Mo 3d and S 2s region; D: S 2p region)

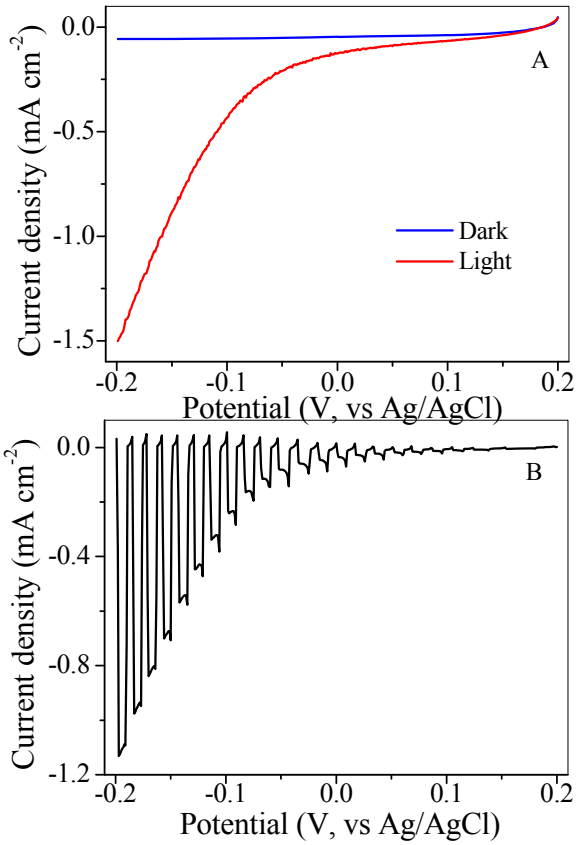


**Fig. 2** (A) Linear sweep voltammagrams of the $MoS_3$/SiNW electrode, the scan rate was 100 mV $s^{-1}$; (B) The transient current responses to on-off cycles of illumination on photocathodes at applied potentials from -0.2 to 0.2 V vs Ag/AgCl with Pt as the counter electrode, the scan rate was 10 mV $s^{-1}$

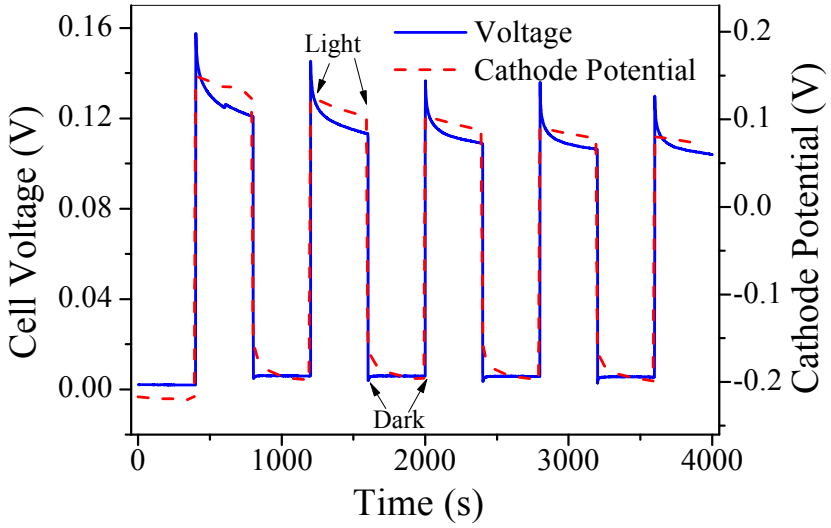


**Fig. 3** Performance of the light-induced BPEC (52.4 Ω of resistor) and photocathode potential change under chopped light illumination

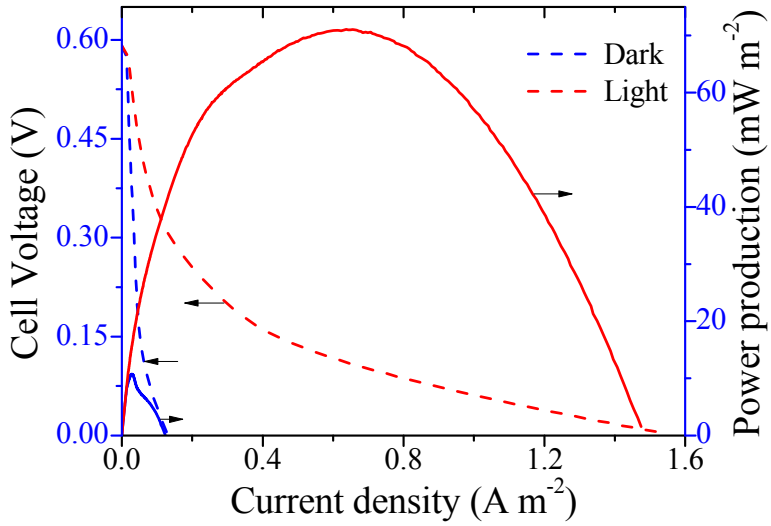


**Fig. 4** Polarization (dash line) and power density (solid line) curves of the BPEC in dark (blue curve) and light (red curve), respectively. Polarization curves were determined by performing linear sweep voltammetry with a two-electrode system in one typical cycle. The scan rate was 1 mV $s^{-1}$.

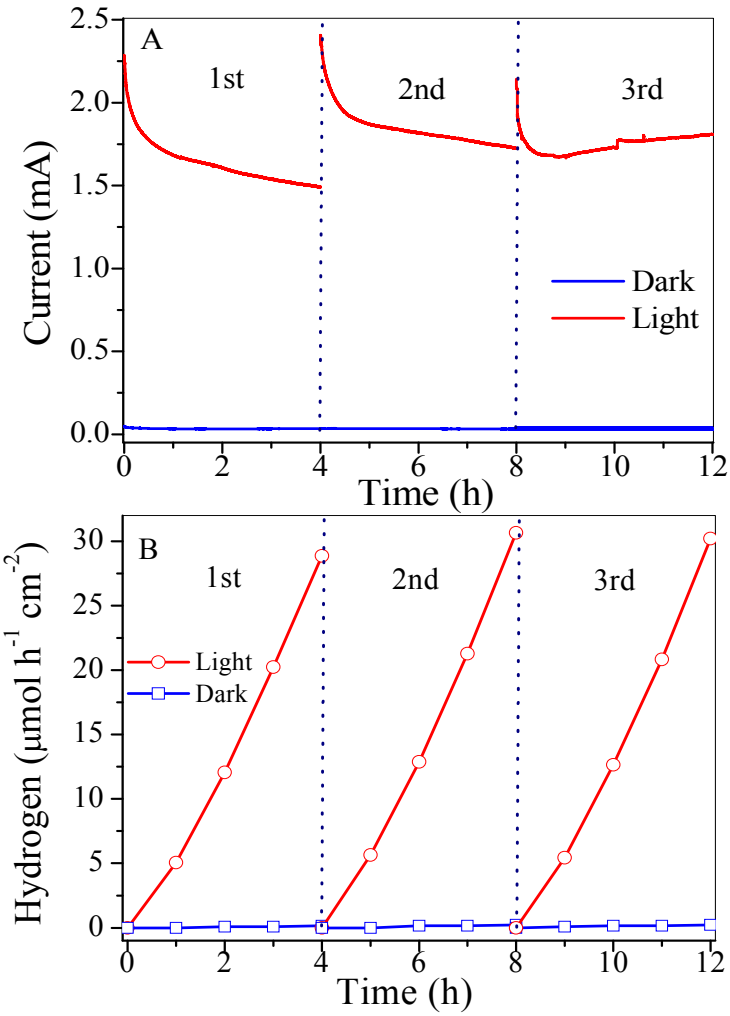


**Fig. 5** Current (A) and hydrogen production (B) of the BPEC (across 52.4 Ω resistor) in dark and light.

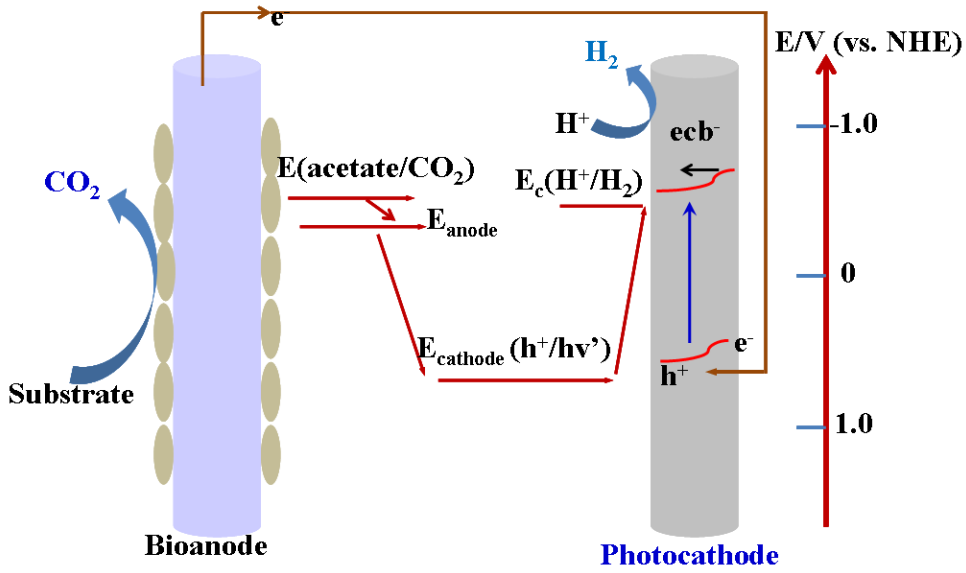


**Fig. 6** Working principle of the BPEC